

Resolution and Synthetic Aperture Characterization of Sparse Radar Arrays

NATHAN A. GOODMAN, Member, IEEE

JAMES M. STILES, Senior Member, IEEE
University of Kansas

The concept of radar satellite constellations, or clusters, for synthetic aperture radar (SAR), moving target indicator (MTI), and other radar modes has been proposed and is currently under research. These constellations form an array that is sparsely populated and irregularly spaced; therefore, traditional matched filtering is inadequate for dealing with the constellation's radiation pattern. To aid in the design, analysis, and signal processing of radar satellite constellations and sparse arrays in general, the characterization of the resolution and ambiguity functions of such systems is investigated. We project the radar's received phase history versus five sensor parameters: time, frequency, and three-dimensional position, into a phase history in terms of two eigensensors that can be interpreted as the dimensions of a two-dimensional synthetic aperture. Then, the synthetic aperture expression is used to derive resolution and the ambiguity function. Simulations are presented to verify the theory.

Manuscript received December 29, 2001; revised November 19, 2002 and April 7, 2003; released for publication April 7, 2003.

IEEE Log No. T-AES/39/3/818501.

Refereeing of this contribution was handled by L. M. Kaplan.

This work was supported in part by the Air Force Office of Scientific Research under Contract F49620-99-1-0172.

Authors' current addresses: N. A. Goodman, Dept. of Electrical and Computer Engineering, University of Arizona, 1230 E. Speedway Blvd., Tucson, AZ 85721-0104, E-mail: (goodman@ece.arizona.edu); J. M. Stiles, Radar Systems and Remote Sensing Laboratory, The University of Kansas, Lawrence, KS 66045.

0018-9251/03/\$17.00 © 2003 IEEE

I. INTRODUCTION

As evidenced by recent literature [1–4] and by the theme of a recent radar conference, *2001: Radar's Odyssey into Space* [5], there is currently much interest in moving radar technology onto spaceborne platforms. The advantages of moving radar into space are numerous [3, 6–7]. First, spaceborne radars provide global coverage, as opposed to airborne radars that are limited by airspace restrictions. Satellite radars may also reduce the amount of personnel needed to support surveillance operations, since no on-board crew is necessary. Furthermore, support personnel and the radar asset are not as vulnerable to military threats as they would be on an airborne platform.

One proposed concept for a space-based radar (SBR) system is to place multiple transmitters and receivers into space, each on their own, small satellite [8–11]. These satellites, called microsats, would fly in a formation called a satellite constellation. Each satellite in the constellation would be able to coherently sample the signal transmitted from each of the transmitters in the constellation. In this way, the constellation would work as a single, virtual radar able to operate in multiple modes including interferometric, synthetic aperture radar (SAR), and moving target indicator (MTI).

The advantages of a microsat constellation are numerous [2, 8–9, 12–14]. First, it may be less expensive to launch several microsats than to launch a large satellite with the same overall antenna aperture due partly to the possibility of using microsats to optimize a launch vehicle's payload capacity. Manufacturing costs are also reduced through the benefits of mass production. In addition, a microsat constellation degrades gracefully as individual microsats fail, either as expected or prematurely, and the constellation can be reconfigured to optimize its configuration after a failure [15]. Failure in a monolithic satellite, however, is catastrophic for the entire radar system. When microsat failure causes system performance to fall below an acceptable level, the hardware and launch costs of a few replacement microsats are much less than an entire replacement system. Furthermore, microsat replacement can be stretched out over time as funding becomes available, and system upgrades can be performed by either replacing failed microsats or augmenting constellations with new, upgraded microsats.

The main disadvantage of a microsat constellation is that the constellation will constitute a sparsely populated, nonuniform, three-dimensional array. Although planar, regularly spaced, tightly packed satellite clusters have been discussed, the fuel requirements for maintaining such a constellation are prohibitive. Consequently, radar signal processing algorithms previously developed for SAR and MTI are not applicable. The traditional

displaced-phase-center-antenna (DPCA) and space-time adaptive processing (STAP) algorithms assume uniform, linear arrays aligned along the direction of travel and have been applied primarily to sidelooking scenarios. For example, the Joint Surveillance Target Attack Radar System (JSTARS) uses a 24 ft phased array in along-track that is mechanically scanned in cross-track [3, 16]. The microsat constellation, therefore, amounts to a unique challenge for radar engineers. New algorithms must be developed to accommodate the unique array structure and wide range of look geometries that will be encountered.

Before effective algorithms can be developed, however, a method for analyzing important system characteristics must be established. Specifically, the constellation's resolution and ambiguity function must be determined. The importance of these parameters is obvious for SAR, but also has significance for MTI because they determine clutter rank, which is a measure of the degrees of freedom in the collected data used up by ground clutter. The radar system's resolution and ambiguity function will depend on five sensor parameters: time, frequency, and three-dimensional spatial location. Resolution and ambiguity are typically determined by coherent processing interval (CPI) and signal bandwidth, but this may not be the case for large constellations that have very small spatial beamwidths. Characterizing a constellation's resolution and ambiguity function as determined by the sensor's five parameters, therefore, is a critical step in determining if SAR and MTI are achievable for a given microsat constellation and in developing appropriate signal processing algorithms.

The rest of this paper is dedicated to characterizing a 3D satellite constellation's resolution and ambiguity function. In Section II, we describe the radar model, including system geometry, and derive the phase of the received signal as a function of the five sensor parameters. In Section III, we derive a transformation that projects the 5D sample structure into a 2D synthetic aperture. The 2D synthetic aperture is analogous to the along-track synthetic aperture that is the well-understood interpretation of SAR. In Section IV, we use the synthetic aperture to determine the constellation's resolution and ambiguity function, and we also present simulation results to confirm the theory. We make our conclusions in Section V.

II. RADAR MODEL

The assumed radar geometry is shown in Fig. 1. The spaceborne system travels in the positive x -direction at velocity v , and the array phase reference at time zero is located at the origin of the coordinate system. Therefore, assuming a flat Earth, the z -coordinate of all targets on the ground is $-h$, where h is the altitude of the array phase reference.

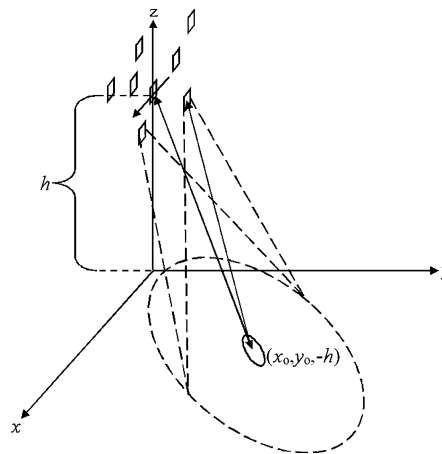


Fig. 1. Radar geometry for constellation of radar satellites.

For this paper we consider a single transmit element surrounded by multiple, isotropic receive elements. The path traveled by the transmit element passes through the coordinate system origin at time zero.

From Fig. 1, the vector defining the position of a spot on the Earth's surface \mathbf{x} is given by $\mathbf{x} = [x \ y \ -h]^\dagger$ where $(\cdot)^\dagger$ denotes the matrix or vector transpose operation. Since the transmitter is located at the array phase reference, which passes through the origin at time $t = 0$, its position at any given time is $\mathbf{r}_t = \mathbf{v}t$ where \mathbf{v} is the radar system's velocity vector, $\mathbf{v} = [v \ 0 \ 0]^\dagger$. The location of a receiver at $t = 0$ is defined as $\mathbf{r} = [r_x \ r_y \ r_z]^\dagger$.

The complex signal d at the output terminals of a receiving antenna due to a stationary scatterer depends on the field intensity pattern of the transmitter $g(\mathbf{x})$, the inverse of the square of the scatterer's range $R(\mathbf{x})$, the two-way propagation delay $\tau(\mathbf{x}, \mathbf{r}, t)$, the scatterer's reflection coefficient $\gamma(\mathbf{x})$, and on the sensor's five measurement parameters. We assume here that the scatterer's reflection coefficient does not vary with time, frequency, or aspect angle. Therefore, the received signal due to a single scatterer is

$$d(\mathbf{x}, \mathbf{r}, \omega, t) = \frac{\gamma(\mathbf{x})g(\mathbf{x})}{R(\mathbf{x})^2} w(\mathbf{r}, \omega, t) \exp[-j\omega\tau(\mathbf{x}, \mathbf{r}, t)] \quad (1)$$

where ω is angular frequency and $w(\mathbf{r}, \omega, t)$ is a weight function describing the sensor response across the measurement parameters of time, frequency, and space. For example, the behavior of $w(\mathbf{r}, \omega, t)$ versus frequency describes the bandwidth of the transmit signal and the sensor's receiver. Letting the sensor measurement parameters be represented by a single vector, $\mathbf{s} = [\mathbf{r}^\dagger \ \omega \ t]^\dagger$, the phase of (1) is represented by

$$\Psi(\mathbf{x}, \mathbf{s}) = \omega\tau(\mathbf{x}, \mathbf{r}, t), \quad (2)$$

and the received signal response in (1) is

$$d(\mathbf{x}, \mathbf{s}) = \frac{\gamma(\mathbf{x})g(\mathbf{x})}{R(\mathbf{x})^2} w(\mathbf{s}) \exp[-j\Psi(\mathbf{x}, \mathbf{s})]. \quad (3)$$

From (3), it is apparent that several variables affect the phase of the received radar response due to a single scatterer. The phase varies with sensor time, space, and frequency as well as the location of the scatterer. The only scatterer-dependent parameters that affect how the received phase varies are the x and y coordinates of the scatterer. Since the scatterers only have two variables that affect their response at the radar, it is reasonable to assume that only two sensor dimensions are needed for representing the SAR data. Therefore, the hypothesis is that although the phase expression of (3) varies versus five sensor parameters, those sensor parameters can be projected into the coordinates of two independent eigensensors. The projection of a sensor's time, space, and frequency parameters onto these two eigensensors forms a 2D synthetic sensor that can be used to characterize SAR and MTI performance. We further note that although a flat-Earth approximation has been made here, a 2D synthetic aperture can be generated for stationary scatterers located on any 2D surface because only two independent variables are needed to define a scatterer's location.

III. SPACE-TIME-FREQUENCY SYNTHETIC APERTURE

The manner in which Ψ varies over scatterer position and sensor parameters determines resolution and the radar ambiguity function. For sidelooking arrays with large bandwidths, long CPI lengths, and relatively small physical arrays, the along-track and cross-track directions decouple and we understand very well the resulting along-track and cross-track resolutions [17]. For the microsat concept, however, this may not be the case. Even for sidelooking geometries, if the physical array is wide enough that the mainlobe of the array pattern dominates resolution rather than bandwidth and CPI length, then the two main axes of resolution may rotate away from along- and cross-track. Furthermore, the satellite constellation may be steered to look forward or backward. In this case, the size and orientation of the resolution cell are not straightforward to determine. We need a method of predicting the ambiguity function and size and shape of a resolution cell for a wide range of transmitted signals, physical arrays, and look geometries.

In this section, we derive a method for determining a radar system's resolution and ambiguity function. We expand the received phase response using Taylor expansions to demonstrate that the five sensor parameters of space, time, and frequency can be projected into an equivalent two-dimensional sensor that we call the 2D synthetic aperture. The 2D synthetic aperture is analogous to the 1D synthetic aperture interpretation of traditional SAR. In SAR, one or more receivers are placed on a moving platform. As the platform moves over successive

samples, the measurements obtained are equivalent to a set of measurements obtained by a nonmoving array with element spacing dependent on the pulse repetition interval (PRI); hence, time and along-track position are related by the sensor velocity. More generally, however, we can say that two sensor parameters, time and along-track position, are transformed into an equivalent 1D aperture. Similarly, we take five sensor parameters and project them into a 2D synthetic aperture. The advantage is the same as for traditional SAR. We analyze the synthetic aperture to understand the resolution and ambiguity function of the moving radar system. Here, we use the 2D synthetic aperture to understand the resolution and ambiguity function of a radar system that moves with time, samples over a certain bandwidth, and has receive elements offset in along-track and two cross-track dimensions.

A. Synthetic Aperture Derivation

First-order Taylor expansions of the phase of the radar response are performed in two steps. First, Ψ is expanded around the radar sensor parameters \mathbf{s} . The result is

$$\Psi(\mathbf{x}, \mathbf{s}) \approx \Psi(\mathbf{x}, \bar{\mathbf{s}}) + (\nabla_{\mathbf{s}} \Psi|_{\mathbf{x}, \bar{\mathbf{s}}})^{\dagger} \Delta \mathbf{s} \quad (4)$$

where

$$\left. \begin{aligned} \bar{\mathbf{s}} &= [r_{x0} \ r_{y0} \ r_{z0} \ \omega_0 \ t_0]^{\dagger} \\ \nabla_{\mathbf{s}} &= [\partial/\partial r_x \ \partial/\partial r_y \ \partial/\partial r_z \ \partial/\partial \omega \ \partial/\partial t]^{\dagger} \\ \Delta \mathbf{s} = \mathbf{s} - \bar{\mathbf{s}} &= [r_x - r_{x0} \ r_y - r_{y0} \ r_z - r_{z0} \ \omega - \omega_0 \ t - t_0]^{\dagger} \end{aligned} \right\} \quad (5)$$

In (4), $\bar{\mathbf{s}}$ is the set of sensor parameters around which the expansion is performed. Using the array phase reference, mean sensor time, and mean frequency, the sensor parameters around which the expansion is performed are given by

$$\bar{\mathbf{s}} = [0 \ 0 \ 0 \ \omega_0 \ 0]^{\dagger}. \quad (6)$$

The first term in (4) is a constant phase term with respect to changes in the sensor parameters, $\Delta \mathbf{s}$. As such, we can assume without a loss of generality that it is zero. The second term of (4) contains all the measurement information about a target at \mathbf{x} . To see this, we explicitly write the derivatives implied by the gradient operation:

$$\begin{aligned} \Psi(\mathbf{x}, \mathbf{s}) &= \frac{\partial \Psi}{\partial r_x} \Big|_{\mathbf{x}, \bar{\mathbf{s}}} r_x + \frac{\partial \Psi}{\partial r_y} \Big|_{\mathbf{x}, \bar{\mathbf{s}}} r_y + \frac{\partial \Psi}{\partial r_z} \Big|_{\mathbf{x}, \bar{\mathbf{s}}} r_z \\ &+ \frac{\partial \Psi}{\partial \omega} \Big|_{\mathbf{x}, \bar{\mathbf{s}}} (\omega - \omega_0) + \frac{\partial \Psi}{\partial t} \Big|_{\mathbf{x}, \bar{\mathbf{s}}} t. \end{aligned} \quad (7)$$

The derivatives in the first three terms show the change of measurement phase with respect to sensor

position in each of three spatial directions. These are, by definition, the spatial frequencies $k_x(\mathbf{x})$, $k_y(\mathbf{x})$, and $k_z(\mathbf{x})$ of the wave scattered from a target at \mathbf{x} . Likewise, the fourth term provides the change in measurement phase with respect to temporal frequency, which is the definition of the propagation delay to the target. The final term shows the change in measurement phase as a function of time, which defines the target's Doppler frequency. Recognizing these definitions, (7) can be written as

$$\begin{aligned} \Psi(\mathbf{x}, \mathbf{s}) &= k_x(\mathbf{x})r_x + k_y(\mathbf{x})r_y + k_z(\mathbf{x})r_z \\ &+ \tau(\mathbf{x})(\omega - \omega_0) + \omega_D(\mathbf{x})t \end{aligned} \quad (8)$$

where k_x , k_y , and k_z are the spatial frequencies, τ is the delay, and ω_D is the Doppler frequency associated with the scattered signal from a target at \mathbf{x} . Hence, we can view a radar as a sensor that collects measurements across five dimensions: space, time, and frequency, providing information about five scattered signal frequencies: k_x , k_y , k_z , τ , and ω_D .

Returning to (4), which was the phase function after expanding around the sensor parameters, the sensor-dependent component of phase is written as

$$\Psi(\mathbf{x}, \mathbf{s}) = \mathbf{k}_s(\mathbf{x})^\dagger \Delta \mathbf{s} \quad (9)$$

where $\mathbf{k}_s(\mathbf{x}) = \nabla_s \Psi|_{\bar{\mathbf{x}}, \bar{\mathbf{s}}}$ is used to emphasize similarity with the standard wavenumber vector. Next, the first-order Taylor expansion of $\mathbf{k}_s(\mathbf{x})^\dagger$ around the position of the scatterer on the ground is performed. Defining $\bar{\mathbf{x}} = [x_0 \ y_0 \ -h]^\dagger$ as the central point of illumination on the ground and the point around which the expansion is performed, the expansion is

$$\mathbf{k}_s(\mathbf{x})^\dagger \approx \mathbf{k}_s(\bar{\mathbf{x}})^\dagger + \Delta \mathbf{x}^\dagger [\nabla_x \mathbf{k}_s(\mathbf{x})^\dagger]_{\bar{\mathbf{x}}} \quad (10)$$

where

$$\Delta \mathbf{x} = \mathbf{x} - \bar{\mathbf{x}} = [x - x_0 \ y - y_0]^\dagger \quad (11)$$

and

$$\nabla_x = [\partial/\partial x \ \partial/\partial y]^\dagger. \quad (12)$$

The received phase then becomes

$$\begin{aligned} \Psi(\mathbf{x}, \mathbf{s}) &\approx \mathbf{k}_s(\bar{\mathbf{x}})^\dagger \Delta \mathbf{s} + \Delta \mathbf{x}^\dagger [\nabla_x \mathbf{k}_s(\mathbf{x})^\dagger]_{\bar{\mathbf{x}}, \bar{\mathbf{s}}} \Delta \mathbf{s} \\ &= [(\mathbf{k}_s^0)^\dagger + \Delta \mathbf{x}^\dagger \Lambda_s] \Delta \mathbf{s} \end{aligned} \quad (13)$$

where $\mathbf{k}_s^0 = \mathbf{k}_s(\bar{\mathbf{x}}) = \nabla_s \Psi|_{\bar{\mathbf{x}}, \bar{\mathbf{s}}}$, and $\Lambda_s = \nabla_x (\nabla_s \Psi)^\dagger|_{\bar{\mathbf{x}}, \bar{\mathbf{s}}}$ is coined the sensor transformation matrix. In (13), \mathbf{k}_s^0 is a five-dimensional vector describing the center signal frequencies. These are the average frequency values of the scattered signals from across the illuminated area and correspond to the signal frequencies due to the center location $\bar{\mathbf{x}}$. Therefore, the second term in (13), $\Delta \mathbf{x}^\dagger \Lambda_s$, is a vector that represents the deviation from the center signal frequencies, resulting from a target located at $\bar{\mathbf{x}} + \Delta \mathbf{x}$. The matrix Λ_s thus transforms

the two-dimensional target position vector \mathbf{x} into the five-dimensional scattered signal frequency vector that corresponds to that target.

Using (13), the received signal in (3) becomes

$$d(\mathbf{x}, \Delta \mathbf{s}) = \frac{\gamma(\mathbf{x})g(\mathbf{x})}{R(\mathbf{x})^2} w(\Delta \mathbf{s}) \exp\{-j[(\mathbf{k}_s^0)^\dagger \Delta \mathbf{s} + \Delta \mathbf{x}^\dagger \Lambda_s \Delta \mathbf{s}]\}. \quad (14)$$

Next, attention is turned to the radiation pattern $g(\mathbf{x})$ of the transmitting antenna. The transmitting antenna is a single aperture that is much smaller than the volume spanned by the sparse receive array. For microsat constellations, this corresponds to having only one satellite transmitting. The antenna pattern is given by

$$g(\mathbf{x}) = \int_{S_A} w_l(\mathbf{l}) \exp[-j\Psi_l(\mathbf{x}, \mathbf{l})] d\mathbf{l}. \quad (15)$$

In (15), $w_l(\mathbf{l})$ is the antenna's complex current or field distribution, $\mathbf{l} = [l_x \ l_y \ l_z]^\dagger$ is a vector to a point on the antenna's conducting structure or aperture, S_A is the surface of the conducting structure or aperture, and $\Psi_l(\mathbf{x}, \mathbf{l})$ is the relative phase shift over the antenna due to a slightly varying range to the scatterer location \mathbf{x} . The phase shift $\Psi_l(\mathbf{x}, \mathbf{l})$ is given by

$$\Psi_l(\mathbf{x}, \mathbf{l}) = \frac{\omega_0}{c} |\mathbf{l} - \mathbf{x}|. \quad (16)$$

Since the antenna distribution $w_l(\mathbf{l})$ is complex, it can be written as

$$w_l(\mathbf{l}) = |w_l(\mathbf{l})| \exp[-j\Psi_a(\mathbf{l})]. \quad (17)$$

The phase in (15) is similar to the phase used previously to derive the sensor response. The range to a point \mathbf{x} on the scattering surface varies slightly over the antenna structure. The radiation pattern is obtained by integrating this variation over the antenna structure as indicated by (15). Performing Taylor expansions similar to those performed earlier for the sensor parameters, the phase of the antenna distribution can be expressed as

$$\Psi_l(\mathbf{x}, \mathbf{l}) = (\mathbf{k}_l^0)^\dagger \Delta \mathbf{l} + \Delta \mathbf{x}^\dagger \Lambda_l \Delta \mathbf{l} \quad (18)$$

where

$$\mathbf{k}_l^0 = \nabla_l \Psi_l|_{\bar{\mathbf{x}}, \bar{\mathbf{l}}}, \quad (19)$$

$$\Lambda_l = \nabla_x (\nabla_l \Psi_l)^\dagger|_{\bar{\mathbf{x}}, \bar{\mathbf{l}}}, \quad (20)$$

$$\nabla_l = [\partial/\partial l_x \ \partial/\partial l_y \ \partial/\partial l_z]^\dagger, \quad (21)$$

$$\Delta \mathbf{l} = \mathbf{l} - \bar{\mathbf{l}}, \quad (22)$$

$\bar{\mathbf{l}}$ is the point on the antenna structure around which the first expansion is performed, and Λ_l is termed the antenna transformation matrix. Using (18),

the transmit pattern is

$$g(\mathbf{x}) = \int_{S_A} |w_l(\mathbf{l})| \exp\{-j[\Psi_a(\mathbf{l}) + (\mathbf{k}_l^0)^\dagger \Delta \mathbf{l} + \Delta \mathbf{x}^\dagger \Lambda_l \Delta \mathbf{l}]\} d\mathbf{l}. \quad (23)$$

Last, the transmitting antenna can be focused on the mean scatterer location $\bar{\mathbf{x}}$ by forcing a phase taper of

$$\Psi_a(\mathbf{l}) = -(\mathbf{k}_l^0)^\dagger \Delta \mathbf{l}. \quad (24)$$

Then, the transmit pattern is

$$g(\mathbf{x}) = \int_{S_A} |w_l(\mathbf{l})| \exp(-j\Delta \mathbf{x}^\dagger \Lambda_l \Delta \mathbf{l}) d\mathbf{l}. \quad (25)$$

B. Synthetic Aperture Interpretation

The performance of a traditional, single-aperture, sidelooking SAR is relative easy to evaluate and understand. a target's position in cross-track is determined from the signal delay, while its along-track position is determined by Doppler. Moreover, the cross-track resolution is determined by the frequency bandwidth of the transmit signal, and the along-track resolution is determined by the processing timewidth, or CPI.

Alternatively, the behavior of proposed sparse-array radars appears difficult to evaluate. These sensors, in general, will not be sidelooking, and the spatial extent of the satellite array can be large enough to affect sensor resolution. As a result, all five signal frequencies may be jointly dependent on both the along-track and cross-track positions of the target. This complex coupling between target position and scattered signal frequencies is demonstrated by the sensor transformation matrix Λ_s . In general, all elements of this matrix will be non-zero, showing that each signal parameter is dependent on each dimension of target position. Accordingly, the sensor provides along-track and cross-track resolutions that are both jointly dependent on frequency bandwidth, CPI, and the spatial size of the 3D array. Resolution will be determined by some or all of these parameters, as opposed to just one. Moreover, resolution will be a function of look angle, so that there exists no simple, direct relationship between sensor resolution and sensor bandwidth, CPI, and array size.

However, analysis of the sensor transformation matrix provides a method for projecting the five signal frequencies and five sensor measurements into a two-dimensional space. We find that these projections are orthogonal, such that each projected measurement corresponds to target position in one of two orthogonal directions. In this manner, a two-dimensional synthetic aperture is constructed from the original five-dimensional set of measurements.

To create this synthetic aperture, we begin by expressing the sensor transformation matrix in terms of its singular value decomposition (SVD), given by

$$\mathbf{U}\mathbf{S}\mathbf{V}^\dagger = \Lambda_s, \quad (26)$$

where

$$\mathbf{U} = [\mathbf{u}_1 \quad \mathbf{u}_2] \quad (27)$$

$$\mathbf{S} = \begin{bmatrix} \sigma_1 & 0 & 0 & 0 & 0 \\ 0 & \sigma_2 & 0 & 0 & 0 \end{bmatrix} \quad (28)$$

and

$$\mathbf{V} = [\mathbf{v}_1 \quad \mathbf{v}_2 \quad \mathbf{v}_3 \quad \mathbf{v}_4 \quad \mathbf{v}_5]. \quad (29)$$

Then, with the SVD explicitly expanded, the received phase is

$$\begin{aligned} \Psi(\mathbf{x}, \mathbf{s}) &\approx (\mathbf{k}_s^0)^\dagger \Delta \mathbf{s} + \sigma_1 (\Delta \mathbf{x}^\dagger \mathbf{u}_1) (\mathbf{v}_1^\dagger \Delta \mathbf{s}) + \sigma_2 (\Delta \mathbf{x}^\dagger \mathbf{u}_2) (\mathbf{v}_2^\dagger \Delta \mathbf{s}) \\ &= (\mathbf{k}_s^0)^\dagger \Delta \mathbf{s} + k_\alpha \alpha + k_\beta \beta \end{aligned} \quad (30)$$

where $k_\alpha = \sigma_1 \Delta \mathbf{x}^\dagger \mathbf{u}_1$, $k_\beta = \sigma_2 \Delta \mathbf{x}^\dagger \mathbf{u}_2$, $\alpha = \mathbf{v}_1^\dagger \Delta \mathbf{s}$, and $\beta = \mathbf{v}_2^\dagger \Delta \mathbf{s}$. The sensor transformation matrix can be interpreted using (30). The basis vectors, \mathbf{v}_1 and \mathbf{v}_2 , for the rows of Λ_s project the five sensor parameters into two independent dimensions of a 2D synthetic aperture, α and β . Based on their interpretation using eigenanalysis, the two dimensions are termed eigensensors. The first eigensensor is obtained through the inner product of the sensor parameter vector $\Delta \mathbf{s}$ with \mathbf{v}_1 , and the second eigensensor is obtained through the inner product of the sensor parameter vector $\Delta \mathbf{s}$ with \mathbf{v}_2 . Consequently, the coordinates of an element in the synthetic aperture are given by $\alpha = \mathbf{v}_1^\dagger \Delta \mathbf{s}$ and $\beta = \mathbf{v}_2^\dagger \Delta \mathbf{s}$. When these two dimensions are used as the measurement dimensions, then they are the only two dimensions needed because they are the only two dimensions with non-zero singular values. The other three dimensions: \mathbf{v}_3 , \mathbf{v}_4 , and \mathbf{v}_5 , are associated with zero singular values, and a change in the position of a scatterer produces no change in the measurements obtained in these three dimensions. Therefore, only the first two dimensions provide information about stationary scatterers, and these two dimensions preserve all the information collected by the sensor in space, time, and frequency.

In addition to preserving all the sensor information in just two dimensions, the two eigensensors are also independent. Therefore, the two eigensensors provide information about two orthogonal frequencies that are obtained through inner products with the basis vectors, \mathbf{u}_1 and \mathbf{u}_2 for the columns of Λ_s . The values of the new spatial frequencies are given by $k_\alpha = \sigma_1 \Delta \mathbf{x}^\dagger \mathbf{u}_1$ and $k_\beta = \sigma_2 \Delta \mathbf{x}^\dagger \mathbf{u}_2$.

The eigensensors provide the opportunity to characterize radar behavior with the same simplicity as with standard, sidelooking SAR. Just as signal delay and Doppler correspond, respectively, to target

cross-track and along-track position, the signal frequencies k_α and k_β correspond, respectively, to target position in orthogonal directions \mathbf{u}_1 and \mathbf{u}_2 . Also, just as target resolution in cross-track and along-track depend, respectively, on sensor bandwidth and CPI, target resolution in \mathbf{u}_1 and \mathbf{u}_2 depend, respectively, on the extent, or width, of sensor measurements α and β .

Note that for an individual antenna, Λ_l performs a function similar to what Λ_s performs for the sensor samples. Λ_l takes any point on the structure of an antenna and projects that point onto a plane. The plane is perpendicular to boresight of the antenna as defined by $\bar{\mathbf{x}}$. Therefore, the antenna transformation matrix Λ_l takes an antenna aperture described in 3D space and transforms it into a 2D antenna that has an equivalent illumination pattern for the region surrounding the point $\bar{\mathbf{x}}$. In addition, Λ_l projects the original spatial frequencies corresponding to the x and y positions of the scatterer to new spatial frequencies that are measured by the primary axes of the equivalent 2D antenna.

C. Sidelooking Example

Although the SVD of Λ_s must generally be performed numerically, a sidelooking sensor geometry provides a case where algebraic expressions of the SVD can be determined. The results describe the known behavior of a sidelooking SAR, and provide support to both the validity and utility of this method. From the geometry and vectors defined earlier, the range from the transmitter to a scatter at \mathbf{x} is given by

$$R_{tx} = |\mathbf{r}_t - \mathbf{x}| = \sqrt{(vt - x)^2 + y^2 + h^2}. \quad (31)$$

Likewise, the range from the scatterer back to a receiver is given by

$$R_{rx} = |\mathbf{r} + \mathbf{v}t - \mathbf{x}| = \sqrt{(r_x + vt - x)^2 + (r_y - y)^2 + (r_z + h)^2} \quad (32)$$

and the two-way propagation delay is

$$\tau(\mathbf{x}, \mathbf{r}, t) = \frac{1}{c} \left[\sqrt{(r_x + vt - x)^2 + (r_y - y)^2 + (r_z + h)^2} + \sqrt{(vt - x)^2 + y^2 + h^2} \right]. \quad (33)$$

In terms of derivatives, Λ_s is given by

$$\Lambda_s = \begin{bmatrix} \frac{\partial^2}{\partial x \partial r_x} & \frac{\partial^2}{\partial x \partial r_y} & \frac{\partial^2}{\partial x \partial r_z} & \frac{\partial^2}{\partial x \partial \omega} & \frac{\partial^2}{\partial x \partial t} \\ \frac{\partial^2}{\partial y \partial r_x} & \frac{\partial^2}{\partial y \partial r_y} & \frac{\partial^2}{\partial y \partial r_z} & \frac{\partial^2}{\partial y \partial \omega} & \frac{\partial^2}{\partial y \partial t} \end{bmatrix} \Psi \Bigg|_{\bar{\mathbf{x}}, \bar{\mathbf{s}}} \quad (34)$$

Substituting (33) and (2) into (34) and evaluating at $\bar{\mathbf{s}}$ and $\bar{\mathbf{x}}$, the sensor transformation matrix becomes

$$\Lambda_s = \frac{\omega_0}{c} \begin{bmatrix} \frac{-(h^2 + y_0^2)}{R_0^3} & \frac{x_0 y_0}{R_0^3} & \frac{-x_0 h}{R_0^3} & \frac{2x_0}{\omega_0 R_0} & \frac{-2v(h^2 + y_0^2)}{R_0^3} \\ \frac{x_0 y_0}{R_0^3} & \frac{-(h^2 + x_0^2)}{R_0^3} & \frac{-y_0 h}{R_0^3} & \frac{2y_0}{\omega_0 R_0} & \frac{2vx_0 y_0}{R_0^3} \end{bmatrix} \quad (35)$$

where $R_0 = \sqrt{h^2 + x_0^2 + y_0^2}$. For sidelooking, $x_0 = 0$, and Λ_s becomes

$$\Lambda_s = \begin{bmatrix} \frac{-1}{R_0} & 0 & 0 & 0 & \frac{-2v}{R_0} \\ 0 & \frac{-h^2}{R_0^3} & \frac{-y_0 h}{R_0^3} & \frac{2y_0}{\omega_0 R_0} & 0 \end{bmatrix}. \quad (36)$$

Substituting (36) back into (13), the phase response is

$$\begin{aligned} \Psi(\mathbf{x}, \mathbf{s}) &= (\mathbf{k}_s^0)^\dagger \Delta \mathbf{s} + \frac{\omega_0}{c} (y - y_0) \\ &\times \left[\frac{2y_0}{\omega_0 R_0} (\omega - \omega_0) - \frac{h^2}{R_0^3} r_y - \frac{y_0 h}{R_0^3} r_z \right] \\ &- \frac{\omega_0}{c} \frac{x}{R_0} (r_x + 2vt) \end{aligned} \quad (37)$$

and (14) becomes

$$\begin{aligned} d(\mathbf{x}, \Delta \mathbf{s}) &= \frac{1}{R(\mathbf{x})^2} w(\Delta \mathbf{s}) \exp[-j(\mathbf{k}_s^0)^\dagger \Delta \mathbf{s}] \\ &\times \exp \left\{ -j \frac{\omega_0}{c} (y - y_0) \left[\frac{2y_0}{\omega_0 R_0} (\omega - \omega_0) - \frac{h^2}{R_0^3} r_y - \frac{y_0 h}{R_0^3} r_z \right] \right\} \\ &\times \exp \left[j \frac{\omega_0}{c} \frac{x}{R_0} (r_x + 2vt) \right] \\ &\times \int_{S_A} |w(\mathbf{l})| \exp(-j \Delta \mathbf{x}^\dagger \Lambda_l \Delta \mathbf{l}) d\mathbf{l}. \end{aligned} \quad (38)$$

Looking at (38), it is seen that the along- and cross-track dimensions contribute independent components. In (38), the first line contains the attenuation due to spreading and the measured phase due to the mean target frequencies. The second line describes the cross-track component, the third line describes the along-track component, and the fourth line accounts for the radiation pattern of the transmitter. Isolating the along-track component and noting that $\omega_0 x / c R_0 \approx k_x$, the along-track component is

$$\rho_x = \exp[k_x (r_x + 2vt)]. \quad (39)$$

Equation (39) is the along-track response commonly used in SAR and MTI analysis. It shows that the along-track spatial frequency component is sampled by a synthetic aperture with elements located at $(r_x + 2vt)$. Consequently, (13) is awarded a degree of confidence based on proper prediction of the along-track component for the sidelooking case. Simulations presented later in this paper demonstrate that (13) is valid for a wide span of scenarios.

IV. SENSOR RESOLUTION AND AMBIGUITY FUNCTION

Now that (13) provides a method for projecting all sensor parameters into a synthetic 2D aperture, it is straightforward to evaluate the radar system's resolution and ambiguity function. The beampattern of the resulting synthetic aperture can be determined in the same manner as any physical aperture, albeit with results in terms of spatial frequencies k_α and k_β . The resulting pattern can be directly projected onto an illuminated surface, along the coordinate system defined by \mathbf{u}_1 and \mathbf{u}_2 . This projection results in the function commonly referred to as the sensor's ambiguity function and effectively displays the correlation of one target's response with the response from targets at all other locations. The sensor characteristics that can be discerned from this function include resolution and target ambiguity, where target ambiguity is manifested as grating lobes and sidelobes.

In the first part of this section, expressions are derived that define the resolution of sparse radar arrays. The efficacy of these expressions is demonstrated by comparing their predictions with ambiguity functions generated from a numeric radar simulator. In the latter section, measurement ambiguity in the form of both grating lobes and sidelobes is addressed.

A. Resolution

Radar resolution is traditionally considered in terms of the correlation between two adjacent targets. This correlation can, of course, be expressed in terms of a matched-filter response; therefore, we begin this analysis by determining the output of a matched filter in the presence of two targets. The filter is matched to the first signal, which is due to a target at $\mathbf{x} = \bar{\mathbf{x}}$. Initially, we assume that the transmit aperture has a Gaussian amplitude taper with size and orientation described by the matrix \mathbf{J}_t and phase taper according to (24), such that

$$w_t(\mathbf{l}) = \frac{1}{(2\pi)^{3/2} \sqrt{|\mathbf{J}_t|}} \exp[-\frac{1}{2} \Delta \mathbf{l}^\dagger \mathbf{J}_t^{-1} \Delta \mathbf{l}] \exp[j(\mathbf{k}_t^0)^\dagger \Delta \mathbf{l}]. \quad (40)$$

The received signal due to a scatterer at $\bar{\mathbf{x}}$ with a scattering coefficient of γ_1 is

$$\begin{aligned} d_1(\bar{\mathbf{x}}, \Delta \mathbf{s}) &= \frac{\gamma_1}{R(\bar{\mathbf{x}})^2} w(\Delta \mathbf{s}) \exp[-j(\mathbf{k}_s^0)^\dagger \Delta \mathbf{s}] \\ &\times \int_{-\infty}^{\infty} \frac{1}{(2\pi)^{3/2} \sqrt{|\mathbf{J}_t|}} \exp[-\Delta \mathbf{l}^\dagger \mathbf{J}_t^{-1} \Delta \mathbf{l}] d\Delta \mathbf{l} \\ &= \frac{\gamma_1}{R(\bar{\mathbf{x}})^2} w(\Delta \mathbf{s}) \exp[-j(\mathbf{k}_s^0)^\dagger \Delta \mathbf{s}] g(\bar{\mathbf{x}}). \end{aligned} \quad (41)$$

The received signal due to a second scatterer located at $\bar{\mathbf{x}} + \Delta \mathbf{x}$ with a scattering coefficient of γ_2 is

$$\begin{aligned} d_2(\bar{\mathbf{x}} + \Delta \mathbf{x}, \Delta \mathbf{s}) &= \frac{\gamma_2}{R(\bar{\mathbf{x}} + \Delta \mathbf{x})^2} w(\Delta \mathbf{s}) \exp[-j(\mathbf{k}_s^0)^\dagger \Delta \mathbf{s}] \\ &\times \exp[-j\Delta \mathbf{x}^\dagger \Lambda_s \Delta \mathbf{s}] \\ &\times \int_{S_A} \frac{1}{(2\pi)^{3/2} \sqrt{|\mathbf{J}_t|}} \exp[-\frac{1}{2} \Delta \mathbf{l}^\dagger \mathbf{J}_t^{-1} \Delta \mathbf{l}] \\ &\times \exp[-j\Delta \mathbf{x}^\dagger \Lambda_t \Delta \mathbf{l}] d\Delta \mathbf{l}. \end{aligned} \quad (42)$$

By completing the square in the integrand of (42), d_2 is

$$\begin{aligned} d_2(\bar{\mathbf{x}} + \Delta \mathbf{x}, \Delta \mathbf{s}) &= \frac{\gamma_2}{R(\bar{\mathbf{x}} + \Delta \mathbf{x})^2} w(\Delta \mathbf{s}) \exp[-j(\mathbf{k}_s^0)^\dagger \Delta \mathbf{s}] \\ &\times \exp[-j\Delta \mathbf{x}^\dagger \Lambda_s \Delta \mathbf{s}] \\ &\times g(\bar{\mathbf{x}}) \exp[-\frac{1}{2} \Delta \mathbf{x}^\dagger \Lambda_t \mathbf{J}_t \Lambda_t^\dagger \Delta \mathbf{x}]. \end{aligned} \quad (43)$$

A filter matched to the response from the first target can be implemented by correlating with the function h_c given by

$$h_c = \frac{R(\bar{\mathbf{x}})^2}{g(\bar{\mathbf{x}})} w(\Delta \mathbf{s})^* \exp[j(\mathbf{k}_s^0)^\dagger \Delta \mathbf{s}]. \quad (44)$$

We assume also that the sensor weight function $w(\Delta \mathbf{s})$ is Gaussian with width and orientation described by the covariance matrix \mathbf{J}_s . Although this assumption appears to be restrictive and unrealistic, we show that this Gaussian assumption leads to a result that is also very accurate for other sensor weight functions. Therefore, the sensor weight function, $w(\Delta \mathbf{s})$, is expressed as

$$w(\Delta \mathbf{s}) = \frac{1}{(2\pi)^{5/4} |\mathbf{J}_s|^{1/4}} \exp(-\frac{1}{4} \Delta \mathbf{s}^\dagger \mathbf{J}_s^{-1} \Delta \mathbf{s}). \quad (45)$$

The output ξ of the correlation filter is

$$\begin{aligned} \xi &= \int_S (d_1 + d_2 + n_i) h_c d\Delta \mathbf{s} \\ &= \gamma_1 \int_S |w(\Delta \mathbf{s})|^2 d\Delta \mathbf{s} \\ &\quad + \gamma_2 \frac{R(\bar{\mathbf{x}})^2}{R(\bar{\mathbf{x}} + \Delta \mathbf{x})^2} \exp[-\frac{1}{2} \Delta \mathbf{x}^\dagger \Lambda_t \mathbf{J}_t \Lambda_t^\dagger \Delta \mathbf{x}] \\ &\quad \times \int_S |w(\Delta \mathbf{s})|^2 \exp[-j\Delta \mathbf{x}^\dagger \Lambda_s \Delta \mathbf{s}] d\Delta \mathbf{s} + n_o \end{aligned} \quad (46)$$

where n_i and n_o are additive Gaussian noise at the input and output of the filter, respectively, and the integrations are performed over the full range of each sensor measurement parameter. The first term in (46) is simply an integration over a 5D Gaussian function; therefore, the integral goes to one and the first term becomes the desired output, γ_1 . Since the filter is

matched to the first scatterer, the second term in (46) depends on the correlation between d_1 and d_2 . The second term, which is temporarily designated as ξ_2 , is

$$\xi_2 = \gamma_2 \frac{R(\bar{\mathbf{x}})^2}{R(\bar{\mathbf{x}} + \Delta\mathbf{x})^2} \exp\left(-\frac{1}{2} \Delta\mathbf{x}^\dagger \Lambda_l \mathbf{J}_l \Lambda_l^\dagger \Delta\mathbf{x}\right) \times \exp\left(-\frac{1}{2} \Delta\mathbf{x}^\dagger \Lambda_s \mathbf{J}_s \Lambda_s^\dagger \Delta\mathbf{x}\right). \quad (47)$$

Noting that

$$\frac{R(\bar{\mathbf{x}})^2}{R(\bar{\mathbf{x}} + \Delta\mathbf{x})^2} \approx 1 \quad (48)$$

when $\Delta\mathbf{x}$ is small, the output of the correlation filter becomes

$$\xi = \gamma_1 + \gamma_2 \exp\left[-\frac{1}{2} \Delta\mathbf{x}^\dagger (\Lambda_s \mathbf{J}_s \Lambda_s^\dagger + \Lambda_l \mathbf{J}_l \Lambda_l^\dagger) \Delta\mathbf{x}\right] + n_o. \quad (49)$$

Equation (49) shows that the output of the correlation filter depends on three terms. The first term is the desired output—the reflectance due to the pixel of interest. The second term is the error due to leakage of the second target into the filter output. It depends on the exponential term, which we now recognize as the correlation between the two scatterers. The last term is the error due to noise that passes through the matched filter.

1) *Resolution Defined by Target Correlation:* We use two criteria for defining sensor resolution. The first uses the more traditional approach where two targets are resolvable if their responses are sufficiently uncorrelated. From (49), the correlation between the responses of targets located at $\bar{\mathbf{x}}$ and $\bar{\mathbf{x}} + \Delta\mathbf{x}$ is

$$\kappa_c = \exp\left[-\frac{1}{2} \Delta\mathbf{x}^\dagger (\Lambda_s \mathbf{J}_s \Lambda_s^\dagger + \Lambda_l \mathbf{J}_l \Lambda_l^\dagger) \Delta\mathbf{x}\right]. \quad (50)$$

We can use this expression to determine the correlation between two targets displaced by $\Delta\mathbf{x}$, or we can fix the correlation κ_c to a specified value and determine the locations of all targets that are correlated by the same amount. Taking the natural logarithm of (50), we get elliptical contours of constant correlation defined by

$$-2 \ln \kappa_c = \Delta\mathbf{x}^\dagger (\Lambda_s \mathbf{J}_s \Lambda_s^\dagger + \Lambda_l \mathbf{J}_l \Lambda_l^\dagger) \Delta\mathbf{x}. \quad (51)$$

If the constant κ_c represents the correlation required for target resolution, then the resulting contour can be considered the resolution ellipse, a contour that indicates both the size and orientation of the mainlobe of the sensor ambiguity function. The size of the ellipse depends on both the value of κ_c and on the resulting matrix in parentheses. For example, the size of the ellipse depends inversely on the matrix's determinant. If the sensor's measurement extent is increased (e.g., its bandwidth and/or CPI is increased), the variances in \mathbf{J}_s become larger, and the determinant of the matrix increases. As a result, the resolution

ellipse decreases in size, indicating an expected improvement in sensor resolution.

Typically, the transmit antenna does not impact radar sensor resolution. Accordingly, the determinant of $\Lambda_l \mathbf{J}_l \Lambda_l^\dagger$ is relatively small, and (51) can be approximated as

$$-2 \ln \kappa_c \approx \Delta\mathbf{x}^\dagger \Lambda_s \mathbf{J}_s \Lambda_s^\dagger \Delta\mathbf{x}. \quad (52)$$

2) Resolution Defined by Estimation Error:

The second approach to resolution is based on the Cramer–Rao lower bound (CRLB). The matched filter output value ξ can be used to estimate the complex reflection coefficient γ_1 . Due to measurement noise and the presence of a second target with unknown reflectance γ_2 , this estimate will exhibit error that depends on the estimator implemented. The CRLB, however, provides a lower bound on the error variance produced by any unbiased estimator.

We begin by determining the Fisher information matrix [18], defined as

$$\mathbf{J} = E\{[\nabla_\gamma(\ln p(\xi | \gamma))][\nabla_\gamma(\ln p(\xi | \gamma))]^\dagger\}. \quad (53)$$

Given that the noise and complex target reflectances can be accurately described as independent Gaussian random variables, \mathbf{J} is determined to be

$$\mathbf{J} = \begin{bmatrix} \frac{1}{\sigma_n^2} + \frac{1}{\sigma_\gamma^2} & \frac{\kappa_c}{\sigma_n^2} \\ \frac{\kappa_c}{\sigma_n^2} & \frac{\kappa_c^2}{\sigma_n^2} + \frac{1}{\sigma_\gamma^2} \end{bmatrix} \quad (54)$$

where $E[|\gamma_1|^2] = E[|\gamma_2|^2] = \sigma_\gamma^2$, $E[\gamma_1 \gamma_2^*] = 0$, and $E[|n_o|^2] = \sigma_n^2$. The CRLB is contained in the inverse of this information matrix,

$$\mathbf{J}^{-1} = \frac{1}{\sigma_n^2 + \sigma_\gamma^2(1 + \kappa_c^2)} \begin{bmatrix} \sigma_\gamma^2(\sigma_n^2 + \sigma_\gamma^2 \kappa_c^2) & -\kappa_c \sigma_\gamma^4 \\ -\kappa_c \sigma_\gamma^4 & \sigma_\gamma^2(\sigma_n^2 + \sigma_\gamma^2) \end{bmatrix}. \quad (55)$$

The lower bounds for the estimation error variance of the two target reflectances are given on the main diagonal of (55). Therefore, the CRLB of the error variance of the estimate $\hat{\gamma}_1(\xi)$ is

$$E[|\gamma_1 - \hat{\gamma}_1(\xi)|^2] \geq \sigma_\gamma^2 \frac{1 + \frac{\sigma_\gamma^2}{\sigma_n^2} \kappa_c^2}{1 + \frac{\sigma_\gamma^2}{\sigma_n^2} (1 + \kappa_c^2)} \equiv \kappa_e^2. \quad (56)$$

We see in (56) that the estimation error depends on the signal-to-noise ratio (SNR) through the ratio $\sigma_\gamma^2/\sigma_n^2$.

From (56), the target correlation in terms of the CRLB is

$$\kappa_c^2 = \frac{\sigma_\gamma^2 \sigma_n^2 - \kappa_e^2 \sigma_\gamma^2 - \kappa_e^2 \sigma_n^2}{\sigma_\gamma^2 (\kappa_e^2 - \sigma_\gamma^2)}. \quad (57)$$

Inserting (50) into (57), we form the following relationship:

$$-\ln \frac{\sigma_\gamma^2 \sigma_n^2 - \kappa_e^2 \sigma_\gamma^2 - \kappa_e^2 \sigma_n^2}{\sigma_\gamma^2 (\kappa_e^2 - \sigma_\gamma^2)} = \Delta \mathbf{x} (\Lambda_s \mathbf{J}_s \Lambda_s + \Lambda_l \mathbf{J}_l \Lambda_l) \Delta \mathbf{x}. \quad (58)$$

For a desired value of estimate error variance, κ_e^2 , the above expression can be solved for $\Delta \mathbf{x}$. The set of all such solutions can be used to map contours of equal error variance, which again will be elliptically shaped. Therefore, (51) and (58) each define a resolution ellipse, providing a graphical indication of sensor resolution. Equation (51) uses target correlation as the resolution criterion whereas (58) uses estimation error variance. Although the target correlation is the more traditional criterion, (58) uses a criterion more directly dependent on sensor parameters, specifically SNR and desired estimate error variance.

3) *Simulations*: Using (51), we have predicted the resolution ellipses for several cases and compared them with ambiguity functions obtained numerically using a multiple aperture radar simulator. The numeric simulator was developed in-house. It computes the in-phase and quadrature analog-to-digital converter samples for a scatterer at a given location \mathbf{x} . The samples are computed for every array element, slow-time sample, and frequency (fast-time) sample. The sets of measurements due to all illuminated scatterers can be weighted by their corresponding scattering reflectivities and summed to obtain a simulated version of the complete radar measurements. Then, the radar measurements can be input into a SAR or MTI processor. In addition, the data samples from each scattering location can be correlated to arrive at a numerically generated ambiguity function. a more detailed description of the simulator is available in [19].

In the first three cases that follow, Gaussian tapers were used for the time and frequency sensor dimensions. a uniform taper, however, was applied across the physical array, with the spatial-dependent elements of \mathbf{J}_s calculated according to a variance measure of the sparse array. For example, the (x, y) component of \mathbf{J}_s , J_s^{xy} , was calculated according to

$$J_s^{xy} = \int_S (r_x - r_{x0})(r_y - r_{y0}) dr_x dr_y. \quad (59)$$

In the fourth example, all five sensor parameters had uniform tapers with elements of \mathbf{J}_s calculated in a manner equivalent to (59).

Fig. 2 shows a sidelooking scenario with a sparse, but relatively small, physical array. The physical array in this case is small enough that the transmit signal's bandwidth and CPI length are the dominant factors in determining resolution. The 2D and 3D views are shown in Figs. 2(a) and 2(b), respectively. The resolution ellipse, shown as black in the 3D view

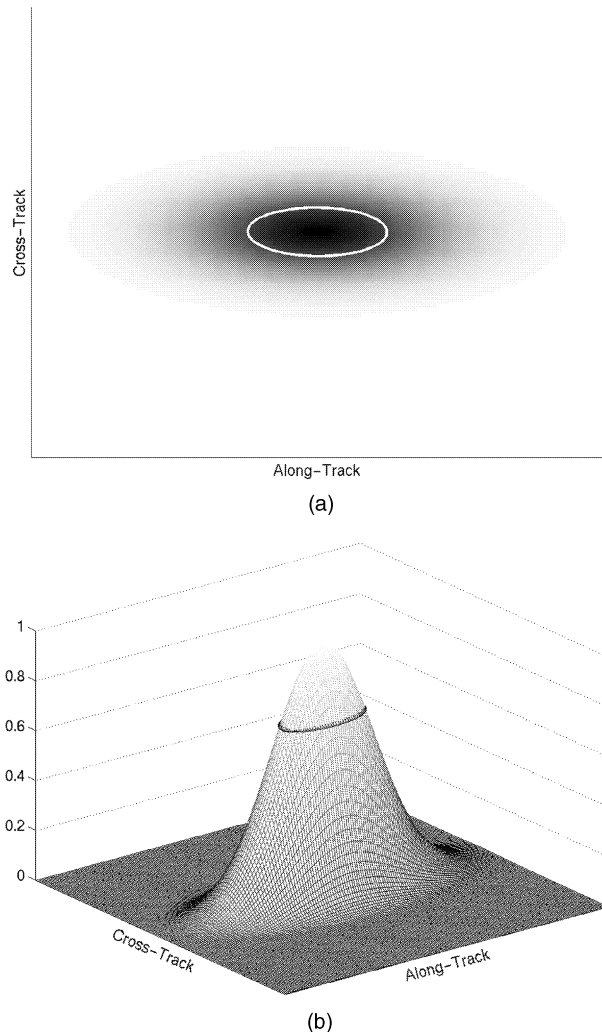


Fig. 2. Simulated ambiguity function and theoretically predicted resolution ellipse for a sidelooking geometry with small physical array. (a) 2D view. (b) 3D view.

and white in the 2D view, is correctly predicted with its axes aligned with the along-track and cross-track directions. The resolution axes align with the along- and cross-track dimensions in this case because resolution is controlled by bandwidth and CPI length. From the 3D view, it is seen that the predicted resolution ellipse intersects the numerical ambiguity function at approximately the specified correlation level, which was $\kappa_c = 0.707$.

When the physical array is extremely large, however, the result is as seen in Fig. 3. In this case, the ellipse becomes smaller because the array beamwidth is smaller than the resolution provided by the sensor's bandwidth and CPI. Moreover, even though the scenario is still sidelooking, the axes of the resolution ellipse rotate away from along- and cross-track because the array formed by the satellite constellation has no along- and cross-track symmetry. In addition, since the physical array is the dominant component and it is sparsely populated with a uniform taper, the sidelobes in the ambiguity function

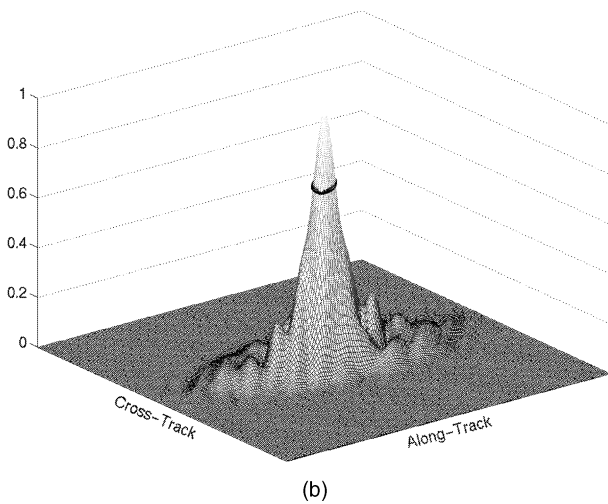
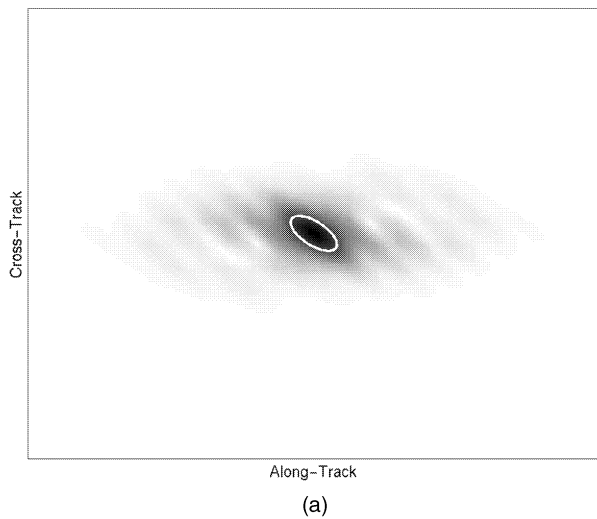


Fig. 3. Simulated ambiguity function and theoretically predicted resolution ellipse for sidelooking geometry with large physical array that affects resolution. (a) 2D view. (b) 3D view.

are much larger in Fig. 3 than they were in Fig. 2.

In Fig. 4, the physical array is again relatively large, but now the scenario is forward looking. The resolution ellipse's size and orientation are correctly predicted by (51). The axes of the resolution ellipse do not align with along- and cross-track because of the forward-looking geometry and the orientation of the satellite array. Sidelobes are again significant because the dominant sensor measurements that determine the mainlobe shape and size are the measurements obtained by the sparse, uniformly weighted, satellite array.

Last, we demonstrate in Fig. 5 that the Gaussian assumption made in deriving (51) is not as restrictive as it may appear. In the simulations that produced Fig. 5, each of the five sensor measurement parameters: time, frequency, and 3D space, were given uniform amplitude tapers. The elements of \mathbf{J}_s were calculated according to the variance of the uniform tapers, as demonstrated for the (x, y) component in (59). The

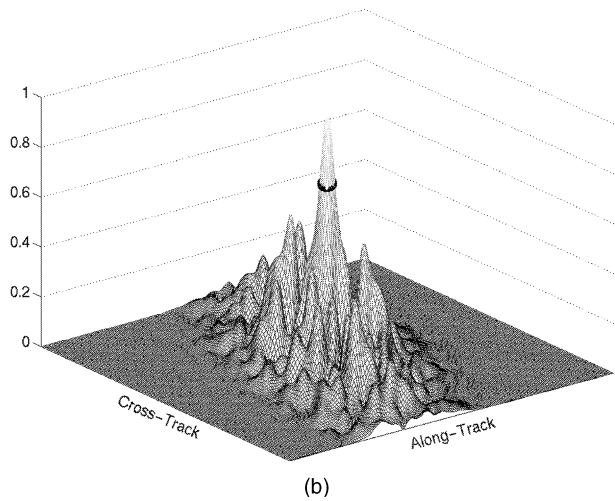
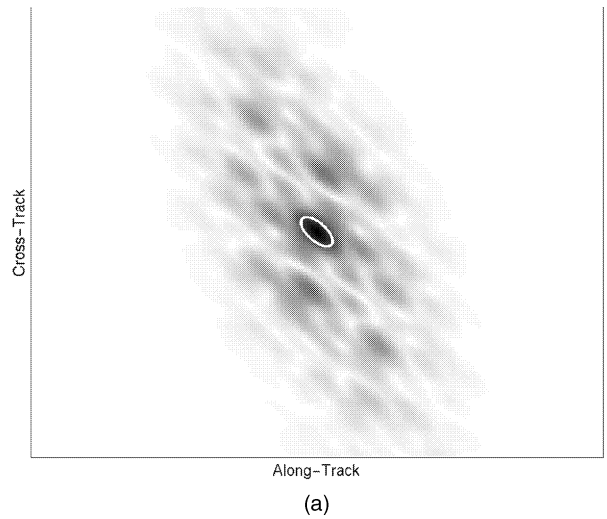


Fig. 4. Simulated ambiguity function and theoretically predicted resolution ellipse for forward-looking geometry with large physical array that affects resolution. (a) 2D view. (b) 3D view.

scenario is forward looking with a moderately sized constellation. Therefore, all five sensor parameters had an effect on total system resolution. The results shown in Fig. 5 demonstrate that by using the variance of the uniform tapers, the resolution of the system can still be determined effectively. Furthermore, since many realistic frequency spectra, time windows, and array functions are closer in shape to a Gaussian taper than to a uniform taper, we conclude that the Gaussian assumption used to derive (51) does not significantly restrict the range of scenarios or sensor functions to which (51) can be applied.

B. Sensor Ambiguity Function

In addition to resolution, a fundamental performance characteristic of a sparse radar array is the sidelobe structure exhibited in the sensor ambiguity function. At a minimum, no grating lobes, which result from perfect measurement correlation between dissimilar targets, should occur within the

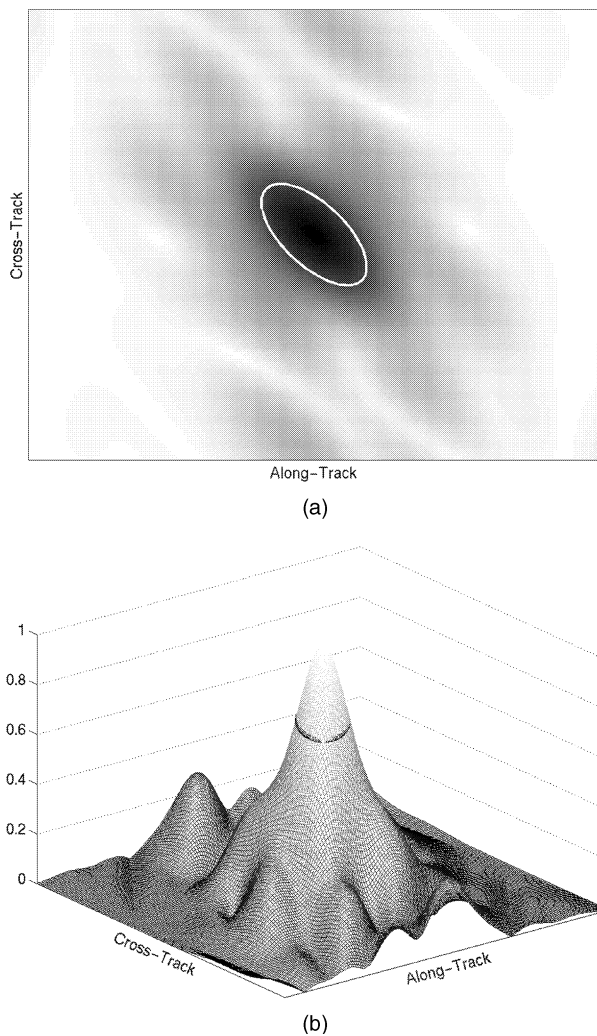


Fig. 5. Simulated ambiguity function and theoretically predicted resolution ellipse for forward-looking geometry with moderately sized physical array that affects resolution. Uniform tapers applied to all five sensor measurement parameters. (a) 2D view. (b) 3D view.

sensor ambiguity function. In addition, the sidelobes of the ambiguity function should ideally be small. Again considering the traditional sidelooking, single-aperture SAR, significant sidelobes within the sensor ambiguity function can be directly determined from knowledge of the transmit pulse repetition frequency (PRF). However, for a sparse radar array, the concept of the synthetic aperture, as discussed in Section III, must be implemented to determine sensor ambiguity. The complexity of this sensor: five sensor measurement parameters, forward- and backward-looking geometries, and the large but sparse spatial array, make a more direct analysis problematic.

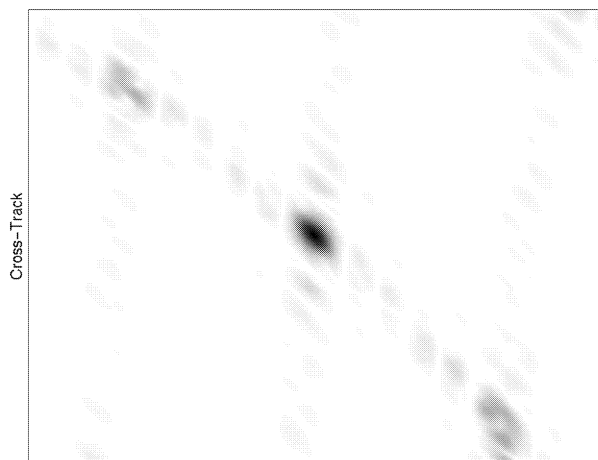
For the analysis in this section, we assume the radar transmits a simple coherent pulse train at a constant PRF. As a result, the sensor weight function for the time parameter $w_t(\Delta t)$ is represented as a periodic series of time samples separated by $1/\text{PRF}$ across the sensor's CPI. Similarly, the weight function

for the frequency parameter $w_f(\Delta\omega)$ is represented as a periodic series of frequency samples separated by $2\pi\text{PRF}$ across the sensor bandwidth. Since the receive array formed by the satellite constellation likewise represents sampling in three dimensions of space, the entire sensor weight function $w(\Delta\mathbf{s})$ represents a five-dimensional array. This array can be then be projected into a two-dimensional synthetic array, using the projection vectors described in Section III.

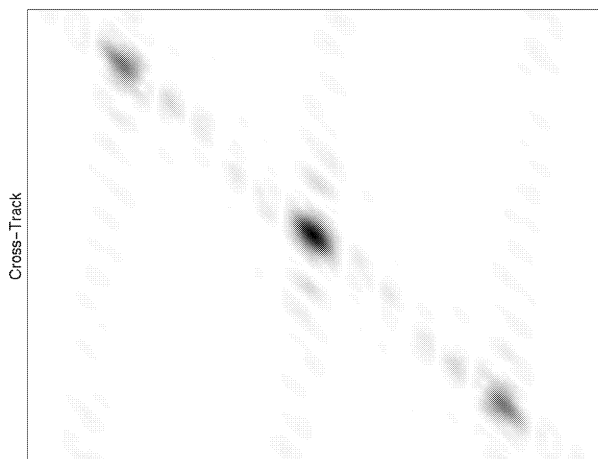
As stated earlier, the sensor ambiguity function for a sparse radar array is determined from the two-dimensional synthetic aperture or array, as described in Section III. As with any aperture or array, the sidelobe levels of the resulting pattern depend on the aperture function since the two are related by a Fourier transform. As a result, the 2D synthetic aperture function of a sparse radar array can provide direct insight into the behavior of this sensor. For example, the size of the aperture in each orthogonal measurement direction will determine sensor resolution. Likewise, to avoid large sidelobes, the aperture or array must be filled—that is, measurements must be made across the entire aperture extent. Additionally, grating lobes can occur if the synthetic aperture or array has periodicities.

More specifically, to evaluate the sidelobe performance of a synthetic array, the concept of a coarray is used. The coarray is the autocorrelation of the array and is a measure of the spatial lags sampled by the array. The far-field power pattern produced by an array is simply the Fourier transform of its coarray. Regularly spaced arrays and coarrays are defined as having spacing that can be laid out on an underlying, evenly spaced grid. Therefore, the distances between samples are always multiples of each other. If samples are missing such that the Nyquist criterion is not satisfied, the array is said to be sparsely populated. If no underlying grid can be found on which to locate the samples, then the array is said to be randomly, or non-uniformly, spaced.

There are two cases where true grating lobes do not occur: when a regularly spaced coarray is Nyquist sampled or when the coarray is irregularly spaced. If a regular coarray results in grating lobes, then their separations from the mainlobe are determined by the minimum separation between coarray samples. Therefore, a regularly spaced, sparse array will not have true grating lobes if some of its coarray samples are closely spaced. For an irregular coarray, high sidelobes are possible, but the lack of a periodic structure prevents true grating lobes. Therefore, a sparse array radar system based on the satellite constellation concept will not likely have true grating lobes, although high sidelobes could be present. For randomly placed arrays such as we have assumed for microsat constellations, the number of apertures in the array strongly controls sidelobe levels. This is because by adding more apertures within the



(a)



(b)

Fig. 6. Comparison of (a) numerically generated ambiguity function with (b) ambiguity function generated using synthetic array.

same constellation area, the sample density of the synthetic array is increased and the result is a more appropriately sampled system. a more detailed discussion of coarrays is available in [20].

First, we demonstrate in Fig. 6 that the synthetic array derived in Section III does, indeed, accurately

predict the sensor's ambiguity function. We generated ambiguity functions for a forward-looking scenario with both our numeric radar simulator and the synthetic array. The ambiguity function obtained from the simulator is shown in Fig. 6(a), and the ambiguity function obtained from the synthetic array is shown in Fig. 6(b). There are some differences in the ambiguity functions since the approximations made in deriving the synthetic array do not apply to the numerical simulation. Specifically, we see that the differences are more apparent at the edges of the ambiguity function. This is because these regions are further from the center of the illuminated area where the second Taylor expansion was performed. However, although there are some differences, the ambiguity functions in Fig. 6a and 6b are generally in good agreement.

Figs. 7 and 8 demonstrate the application of the synthetic coarray. In Fig. 7(a), the 2D synthetic array for a system with a five-element satellite constellation is shown; hence, Fig. 7(a) shows the projection of every physical array element, slow-time sample, and fast-time sample into the 2D eigensensor system. Some periodic samples along dimension α can be seen. These are due to periodic slow-time samples. Likewise, the periodic samples that are seen along dimension β are due to periodic fast-time samples. Additional nonperiodic samples in Fig. 7(a) are due to random array-element spacings projected onto the 2D eigensensor.

In this example, the size of the constellation is relatively small compared with the synthetic aperture spanned by the eight fast-time and eight slow-time samples. Hence, many of the synthetic array samples overlap, and bandwidth and CPI rather than the size of the constellation primarily determine the overall size of the synthetic array. By taking the autocorrelation of the synthetic array, we generate the synthetic coarray shown in Fig. 7(b). Because of the random nature of the spatial sampling, there is no underlying sample grid for either the synthetic array or coarray. Therefore, the corresponding ambiguity function shown in Fig. 7(c) has no true grating lobes.

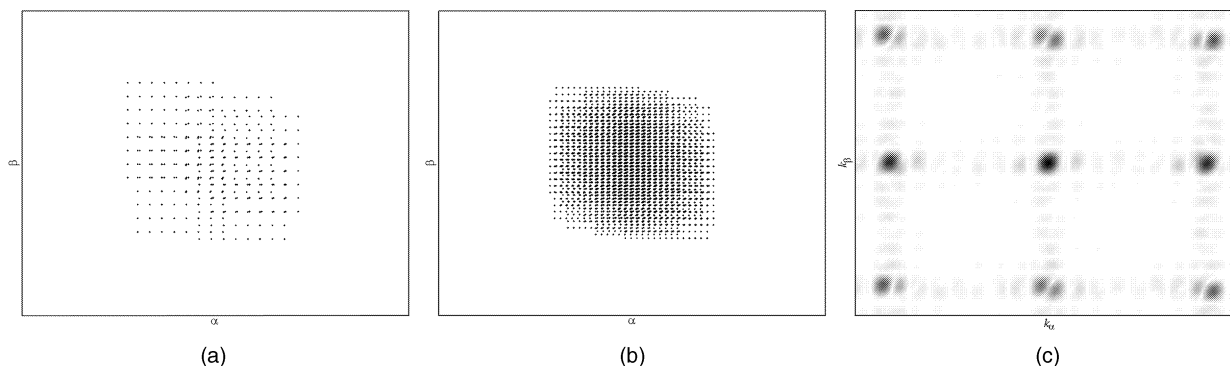


Fig. 7. (a) 2D synthetic array for relatively small constellation generates synthetic coarray in (b). Ambiguity function of system shown in (c).

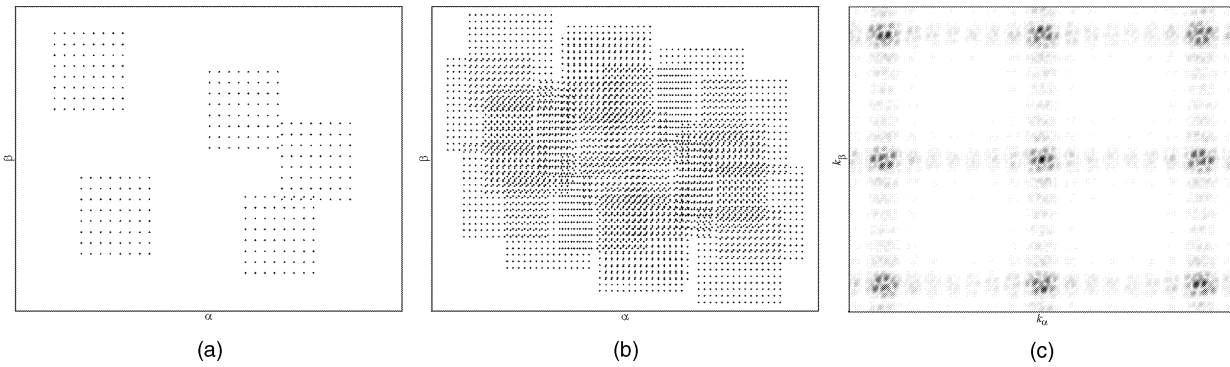


Fig. 8. (a) 2D synthetic array for relatively large constellation generates synthetic coarray in (b). Ambiguity function of system shown in (c).

The random-array ambiguity function, however, does show effects of both the periodic sampling of the radar signal and the sparse, nonperiodic sampling of the satellite constellation. Since there is periodic sampling in both time and frequency, there are hints of range-Doppler ambiguities in the resulting ambiguity function. The potential range-Doppler ambiguities are multiplied by sidelobes of the radar constellation's radiation pattern to arrive at the sidelobes seen in Fig. 7c. Since the array pattern is random in nature, the expected sidelobe levels depend on the sample density in the synthetic array and coarray [20]. This density, in turn, depends on the system PRF, the overall size of the constellation, and the number of satellites in the constellation.

In Fig. 8, we present the results of a final experiment to demonstrate the effect of sample density on the system ambiguity function. The constellation used to generate the results shown in Fig. 7 was relatively small. As a result, many elements of the synthetic array overlapped, the size of the synthetic array was primarily determined by the transmit signal, the density of samples in the synthetic coarray was relatively high, and the sidelobes immediately surrounding the ambiguity function's mainlobe were small. In Fig. 8, however, the satellite constellation is much larger. As a result, the synthetic coarray shown in Fig. 8(a) has wide regions without any samples. The overall size of the synthetic array has increased because of the huge size of the constellation, but the sample density seen in the synthetic coarray of Fig. 8(b) is much less than the density seen in Fig. 7(b). Hence, although resolution has improved through the wider extent of the synthetic array, the reduced sampling density results in high sidelobes immediately surrounding the ambiguity function's mainlobe. The ambiguity function for this case is shown in Fig. 8(c).

The compromise between resolution and sample density is a primary issue for processing of sparse radar arrays. Of course, we desire a high sample density over a wide extent, resulting in good resolution and low sidelobe levels, but this may not be achievable. We can, however, use the simulations

in Figs. 7 and 8 to make some judgments about when sparse arrays can be effectively processed for SAR and MTI. The situation in Fig. 8 is one where resolution has improved through the large size of the constellation. In essence, the number of resolution cells in the SAR map has increased, but the number of measurements for estimating the scattering from those cells has remained constant. Therefore, we cannot expect to be able to perform SAR processing effectively. If, however, we design a system such that bandwidth and CPI are the dominant factors in determining resolution, we ensure a sufficient sampling density such that quality SAR processing is achievable. In other words, the synthetic coarray analysis shows that since the time and frequency measurement dimensions are more sufficiently sampled than the spatial measurement dimensions, they should be the dimensions that largely determine resolution. For extremely wide satellite constellations, this may require very long CPIs and wide signal bandwidths.

V. CONCLUSIONS

There is currently an emphasis on moving radar technology into space, and one proposed concept for doing so is a cooperative constellation of formation-flying micro-satellites. Although there are many advantages to the microsat concept, current signal processing algorithms are, in general, not applicable due to the constellation's sparsely populated physical array. Furthermore, little effort is reported in the literature for dealing with sparsely sampled, irregularly spaced, physical arrays for application to SAR and MTI.

To develop appropriate signal processing algorithms, the ability to describe a radar system's important characteristics is needed. To that end, we have derived a method for quickly and efficiently determining a radar system's resolution and ambiguity characteristics. The technique transforms a radar's full sensor parameters: time, frequency, and spatial position, into a two-dimensional synthetic aperture.

The synthetic aperture's overall size determines its mainlobe width and, therefore, the total system resolution. Also, the synthetic aperture can be used to generate a synthetic coarray that can be used for ambiguity and sidelobe analysis.

A significant advantage of this sensor representation is that it is robust for both forward- and sidelooking scenarios and for both large and small physical arrays. The analysis is valid for fully filled physical arrays as well as sparse arrays. However, since the derivation is based on Taylor expansions, far-field and narrowband conditions are assumed. While these assumptions may be restrictive for very large physical arrays and bandwidths, we have demonstrated through simulation that the synthetic array can be valid for systems where the physical array beamwidth controls resolution rather than bandwidth and coherent integration time. Therefore, based on the 2D synthetic aperture's ability to predict system characteristics over a wide range of sensor structures and look geometries, the method presented in this paper should be a valuable tool for analyzing the performance of radar systems that extend beyond airborne, sidelooking scenarios.

REFERENCES

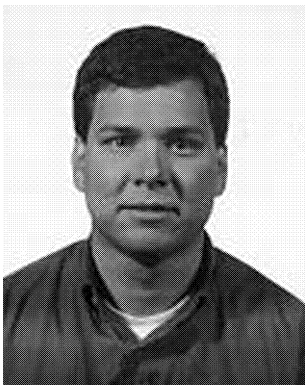
- [1] Scott, W. B. (1999)
Testbeds wring out technologies.
Aviation Week and Space Technology, (Apr. 5, 1999), 52–53.
- [2] Whelan, D. A. (2000)
DISCOVERER II program summary.
In *Proceedings of the IEEE 2000 International Radar Conference*, Washington, D.C., 7–8.
- [3] Entzminger, J., Fowler, C., and Kenneally, W. (1999)
JointSTARS and GMTI: Past, present and future.
IEEE Transactions on Aerospace and Electronic Systems, **35**, 2 (Apr. 1999), 748–761.
- [4] Davis, M. E. (2000)
Technology challenges in affordable space based radar.
In *Proceedings of the IEEE 2000 International Radar Conference*, Washington, D.C., 18–23.
- [5] *Proceedings of the IEEE 2001 Radar Conference*, Atlanta, GA, May 1–3, 2001.
- [6] Overman, K., Leahy, K., and Fritsch, R. J. (2000)
The future of surface surveillance—revolutionizing the view of the battlefield.
In *Proceedings of the IEEE 2000 International Radar Conference*, Washington, D.C., 1–6.
- [7] Nohara, T. J., Weber, P., and Premji, A. (2000)
Space-based radar signal processing baselines for air, land and sea applications.
Electronics & Communication Engineering Journal, **12**, 5 (Oct. 2000), 229–239.
- [8] Zetocha, P., et al. (2000)
Commanding and controlling satellite clusters.
IEEE Intelligent Systems, **15**, 6 (Nov. 2000), 8–13.
- [9] Kitts, C., et al. (1999)
Emerald: A low-cost spacecraft mission for validating formation flying technologies.
In *Proceedings of the 1999 IEEE Aerospace Conference*, Aspen, CO, 217–226.
- [10] Massonnet, D., et al. (2000)
A wheel of passive radar microsats for upgrading existing SAR projects.
In *Proceedings of the IEEE 2000 International Geoscience and Remote Sensing Symposium*, Honolulu, HI, 1000–1003.
- [11] Massonnet, D. (2001)
Capabilities and limitations of the interferometric cartwheel.
IEEE Transactions on Geoscience and Remote Sensing, **39**, 3 (Mar. 2001), 506–520.
- [12] Air Force Research Lab (c. 1999)
TechSat 21 next generation space capabilities.
Available:
www.vs.afrl.af.mil/TechProgs/TechSat21/NGSC.html.
- [13] Martin, M., and Stallard, M. (1999)
Distributed satellite missions and technologies—The TechSat 21 program.
In *Proceedings of the AIAA Space Technology Conference and Exposition*, Albuquerque, NM, Sept. 1999, AIAA 99–4479.
- [14] Das, A., Cobb, R., and Stallard, M. (1998)
TechSat 21: A revolutionary concept in distributed space based sensing.
In *Proceedings of the AIAA Defense and Civil Space Programs Conference and Exhibit*, Huntsville, AL, Oct. 1998, AIAA 98–5255.
- [15] Burns, R., et al. (2000)
Techsat 21: Formation design, control, and simulation.
In *Proceedings of the 2000 IEEE Aerospace Conference*, Big Sky, MT, 19–25.
- [16] Covault, C. (1996)
Joint-Stars patrols Bosnia.
Aviation Week and Space Technology, (Feb. 19, 1996), 44–49.
- [17] N. Levanon (1988)
Radar Principles.
New York: Wiley, 1988.
- [18] Van Trees, H. L. (1968)
Detection, Estimation, and Modulation Theory, Part I.
New York: Wiley, 1968.
- [19] Goodman, N. A. (2002)
SAR and MTI processing of sparse satellite clusters.
Ph.D. dissertation, Dept. of Electrical Engineering and Computer Science, University of Kansas, Lawrence, 2002.
- [20] Johnson, D. H., and Dudgeon, D. E. (1993)
Array Signal Processing: Concepts and Techniques.
Englewood Cliffs, NJ: Prentice-Hall, 1993.



Nathan A. Goodman (S'98—M'02) received the B.S., M.S., and Ph.D. degrees in electrical engineering from the University of Kansas, Lawrence, in 1995, 1997, and 2002, respectively.

He is currently an assistant professor in the Department of Electrical and Computer Engineering at the University of Arizona. From 1996 to 1998, he was an RF systems engineer with Texas Instruments, Dallas, TX, and from 1998 to 2002, he was a graduate research assistant in the Radar Systems and Remote Sensing Laboratory (RSL) at the University of Kansas. His research interests are in radar and array signal processing.

Dr. Goodman was awarded the Madison A. and Lila Self Graduate Fellowship upon returning to the University of Kansas in 1998. He was also awarded the IEEE 2001 International Geoscience and Remote Sensing Symposium Interactive Session Prize Paper Award.



James M. Stiles (S'91—M'95—SM'97) received the B.S. degree in electrical engineering from the University of Missouri, Columbia, in 1983; the M.S. degree in electrical engineering from Southern Methodist University, Dallas, TX, in 1987; and the Ph.D. degree in electrical engineering from the University of Michigan, Ann Arbor, in 1996.

From 1983 to 1990, he was a microwave systems design engineer for Texas Instruments, and from 1990 to 1996 he was employed as a graduate research assistant in the Radiation Laboratory at the University of Michigan. Since 1996, he has been at the University of Kansas, where he is an associate professor of electrical engineering and a member of the Radar Systems and Remote Sensing Laboratory (RSL). His research interests include radar remote sensing of vegetation, propagation and scattering in random media, ground-penetrating radar, and radar signal processing.